GLOBAL-LOCAL FINITE ELEMENT ANALYSIS OF BONDED SINGLE-LAP JOINTS

B. Kilic,* **E. Madenci†**
The University of Arizona, Tucson, AZ 85721

D. R. Ambur,‡
NASA Langley Research Center, Hampton, VA 23681

Abstract

Adhesively bonded lap joints involve dissimilar material junctions and sharp changes in geometry, possibly leading to premature failure. Although the finite element method is well suited to model the bonded lap joints, traditional finite elements are incapable of correctly resolving the stress state at junctions of dissimilar materials because of the unbounded nature of the stresses. In order to facilitate the use of bonded lap joints in future structures, this study presents a finite element technique utilizing a global (special) element coupled with traditional elements. The global element includes the singular behavior at the junction of dissimilar materials with or without traction-free surfaces.

Introduction

Although bonded joints are a primary means for transferring load in the construction of aerospace and marine structures, they are potential failure sites due to the presence of geometric and material discontinuities that cause high stress concentrations. Therefore, the reduction of stress concentrations along the edges of the adhesive is important in order to prevent premature failure of the bonded joint. However, the determination of the complete stress and strain fields in bonded composite lap joints presents difficulties arising from the step-wise geometry, dissimilar material properties, and the effect of stress stiffening (geometrically nonlinear effect) on the bending deformation of the adherends under uniaxial tension. The eccentric loading path may result in bending deflections for a single-lap joint, and the local stress variations near the ends of the overlap region are characterized by very high gradients or even analytically predicted singularities. The sharp gradients of the stress components depend on the elastic properties of the adherends and adhesive, and on the joint geometry. The peak transverse normal (peel) and shear stresses in the adhesive can be reduced by the presence of an overflow of the adhesive toward the edges.

Efforts to understand the mechanisms needed to improve the strength of bonded isotropic and composite materials are ongoing.[1-4] Previous analyses of bonded joints can be categorized as "shear-lag" and "finite-element" approaches. Extensions of the shear-lag model introduced by Goland and Reissner[5] neglect the geometric nonlinearity and the presence of an adhesive overflow at the ends of the overlap. Furthermore, the shear-lag model approximates the transverse shear and normal strain components in terms of the relative displacements of the adherends.

Although finite element models include the complexities arising from certain geometric and dissimilar material details of the structure, they fail to capture the singular stress field at the edges of the adhesive without resorting to sub-modeling. However, a proper aspect ratio between the elements in the adherends and adhesive requires a highly refined mesh, making the finite element analysis computationally challenging. While the stress state in a lap joint is three-dimensional in nature, many finite element models of lap joints were simplified to a two-dimensional analysis under certain assumptions in order to avoid the computational difficulties that arise when performing a mesh refinement.[6-9]

Sub-modeling of the regions near the ends of the overlap was avoided by Barsoum[10-12] using an iterative scheme within the realm of finite element analysis, and without the use of a special element. Ding and Kumosa[13] and Ding et al.[14] applied this method to determine the singular stress field near the intersection of a bimaterial interface with free edges in adhesive joints. Although effective for a bimaterial interface with or without cracks, this approach suffers from the number of iterations required for convergence and the inability to enforce the continuity of traction components across the interface. Also, the rate of convergence and the accuracy of the results are dependent on the material properties and the scaling of

---

*Graduate Research Assistant, Department of Aerospace and Mechanical Engineering.

†Professor, Department of Aerospace and Mechanical Engineering. Member AIAA.

‡ Head, Mechanics and Durability Branch. Associate Fellow AIAA.

the displacements during the iterations. The strength of the singular stress field becomes inaccurate at distances very close to the junction of dissimilar materials; a common location of failure initiation. This inaccuracy may be attributed to the limitation of the finite elements utilized in the analysis.

Both the shear-lag model and finite element models of conventional elements without resorting to sub-modeling fail to capture the singular stress field at the junction of dissimilar materials. However, an alternative to sub-modeling is the global element coupled with conventional finite element analysis introduced by Mote.[15] The extension and application of this method were demonstrated by Lin and Mar,[16] Bradford et al.,[17-19] Dong,[20] Chen,[21] Her,[22] Munz and Yang,[23] Destuynder et al.,[24] Gadi et al.,[25] Pageau and Biggers,[26,27] Akisanya and Fleck,[28] Madenci et al.,[29] Qian and Akisanya,[30] and, more recently, Barut et al.[31]

All of these coupled special elements with built-in leading-order singularity and conventional elements, with exception of the study by Barut et al.,[31] provide results that are dependent on the size of the special element. In order to enhance the accuracy of the results, these enriched elements usually employ transition (overlap) elements, thus introducing another degree of uncertainty as to the extent of the zone for the transition elements. Additionally, inter-element compatibility between the special and conventional elements is not satisfied, except for the special hybrid element by Lin and Mar.[16] Thus, monotonic convergence of the results is not guaranteed. The method introduced by Barut et al. eliminates the aforementioned shortcomings while addressing either an open or a closed junction of multiple dissimilar materials, as shown in Fig. 1. Barut et al. utilized the exact solution for the stress and displacement fields based on the eigenfunction expansion method. The global element for arbitrary geometrical and material configurations is interfaced with conventional elements while satisfying the inter-element continuity. This global element is integrated into the commercially available finite element program ANSYS so that a designer can use the ANSYS pre- and post-processing capabilities and execute the program within the ANSYS environment.

The problem posed herein concerns the singular stress field in the bonded single-lap joint with a square-end fillet, chamfered-end fillet, or spew fillet configuration. The objective is to determine the most critical junction for possible premature failure while including the effect of geometric non-linearity and the presence of a singular stress field at the junctions of dissimilar materials. The numerical results generated in this study concern a bonded single-lap joint with three specific adhesive end overflow configurations. In the first configuration, the adhesive has a square-end fillet without any adhesive overflow. The second configuration has an adhesive with a chamfered-end fillet, and the third has a spew fillet. The global finite element captures the accurate stress distributions in the critical regions of the joint and is capable of extracting the stress intensification parameter. The results from this analysis provide the strain energy density variation required by the failure prediction criterion introduced by Sih and MacDonald[32] that is capable of identifying a potential failure site. Cracks are then located at these sites to represent the damage. The stress intensity factors associated with the crack tips are also captured by using the global elements.

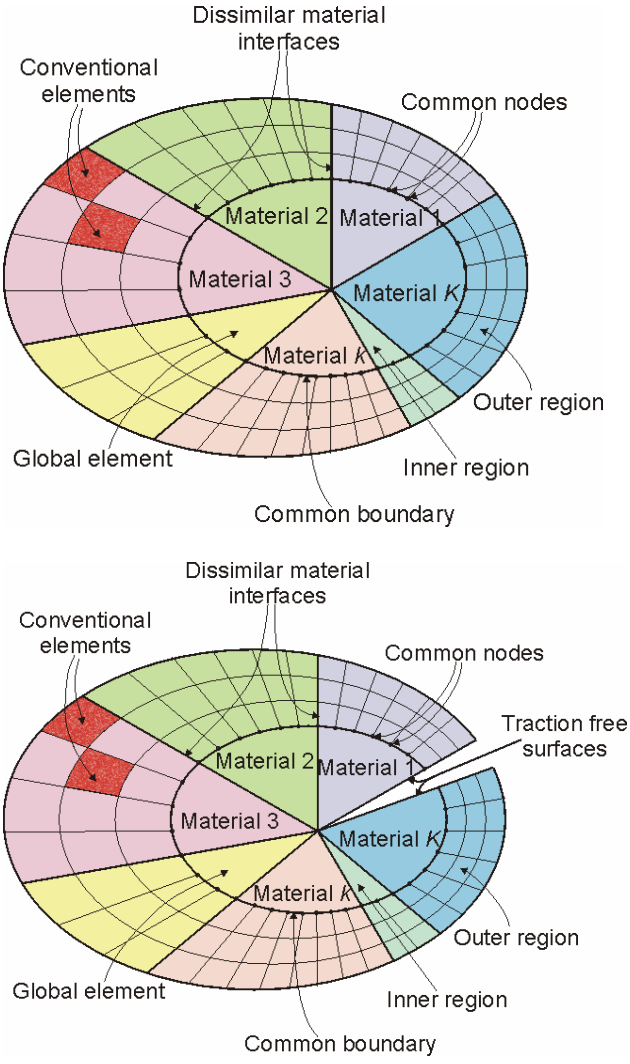

Fig. 1 Conventional elements coupled with a global element for a closed and open junction.

Problem Statement

The geometry and dimensions of the bonded single-lap joints with a square-end fillet, chamfered-end fillet,

or spew fillet configuration, considered previously by Destuynder et al.,[24] are described in Fig. 2.

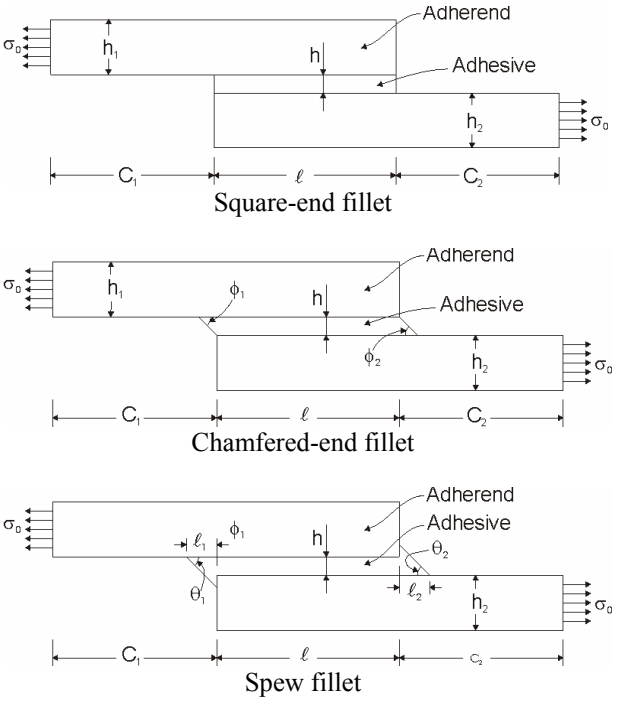

Fig. 2 Typical lap joint configurations: square-end fillet ; chamfered-end fillet ; spew fillet.

The parameters c_1 and c_2 and h_1 and h_2 denote the end distance and thickness of the upper and lower adherends, respectively, with numerical values of $c_1 = c_2 = 90.0$ mm and $h_1 = h_2 = 5$ mm. The overlap length defined by the parameter ℓ is specified as 50 mm. The chamfer is defined by the equal bevel angles of ϕ_1 and ϕ_2 and is specified as 45°. The parameters ℓ_1, ℓ_2, θ_1, and θ_2 describing the spew fillet are specified as $\ell_1 = \ell_2 = 2h$, with the adhesive thickness $h = 0.2$ mm and $\theta_1 = \theta_2 = 45°$. As shown in Fig. 2, the upper and lower adherends are subjected to a uniform stress, $\sigma_0 =$ 1.0 MPa. The adhesive is an isotropic material, with Young's modulus $E = 3.4$ GPa and Poisson's ratio $\nu = 0.35$. The upper and lower adherends are also isotropic, with Young's modulus $E = 200$ GPa and Poisson's ratio $\nu = 0.3$

The finite element discretization with global and conventional elements on each of the adhesive edges in a single-lap joint is illustrated in Fig. 3. As required by the finite element analysis, the rigid-body motion of the lap joints is suppressed by requiring that the loaded ends (surfaces) of the adherends remain perpendicular (i.e., the nodes on these surfaces experience equal displacements) and enforcing zero displacement at the center of the adhesive, $u_x = u_y = 0$. Because the joint width is much greater than the thickness, plane strain conditions prevail. Both the adhesive and the adherends are elastic and exhibit geometrically non-linear elastic behavior.

Solution Method

The solution method combines the global element and conventional elements by modeling the region around the junction with the global element and the area outside this region with conventional elements, as shown in Fig. 1. It provides an accurate description of the singular stress field at the junction of dissimilar materials and geometric discontinuities subjected to general loading conditions. The global-local finite element analysis method developed by Barut et al.[31] is utilized in determining the stress field and the stress intensity factors. As illustrated in Fig. 1, a junction consisting of dissimilar materials is partitioned into inner and outer regions. In the inner region, the presence of a singular stress field near the junction arising from the material and geometric discontinuities requires an exact solution of the governing equations. The solution for the outer region in which a singular stress field does not exist can be constructed by employing the finite element method with conventional elements. Therefore, an accurate solution for the entire domain requires coupling of the exact solution in the inner region with that of the approximate solution through the finite element method in the outer region. This coupling is achieved by developing a global element whose interpolation functions satisfy the governing equations exactly near the junction while enforcing the inter-element displacement continuity along the common boundary and the nodes between the global and conventional elements.

The development of the global element stiffness matrix is similar to that of a conventional element, except for the interpolation functions. These functions are established by solving for the stress and displacement fields in the inner region. Each material is assumed to be elastic, homogeneous, and isotropic with Young's modulus, E_k and Poisson's ratio, ν_k for the k^{th} material. Perfect bonding with zero thickness is assumed along the material interfaces.

As suggested by Williams,[33] the stress and displacement components in the k^{th} material sector are represented by

$$\sigma_{\alpha\beta}^{(k)}(r,\theta) = \sum_{n=0}^{\infty} r^{\lambda_n} F_{\alpha\beta}^{(k)}(\theta;\lambda_n) \tag{1}$$

and

$$u_{\alpha}^{(k)}(r,\theta) = \sum_{n=0}^{\infty} r^{\lambda_n+1} G_{\alpha}^{(k)}(\theta;\lambda_n) \tag{2}$$

with $\alpha, \beta = r, \theta$ ($k = 1, 2, ..., K$), $\lambda_0 = 0$, and $\lambda_n \neq 0$ for $n = 1, 2, ..., N$. The origin of the polar coordinate system (r, θ) coincides with the junction of the vertices. The unknown parameter λ_n depends on the material properties and the geometric configurations, and indicates the strength of the singular behavior for the stress field. As explained in detail by Barut et al.,[31] the explicit forms of the displacement and stress components in the vicinity of the junction are constructed by solving for the equilibrium equations and appropriate interface and boundary conditions.

The stiffness matrix for the global element of dissimilar materials is obtained by considering the total potential. The vector of displacement components along the common boundary between the global element and the conventional elements is expressed in terms of the nodal displacements of the conventional elements. The displacement components along the global element boundary are compatible with those of the conventional elements. Enforcing the first variation of the total potential to vanish results in the nodal equations of equilibrium for the global element. The explicit form of the global stiffness matrix and its validation through existing asymptotic solutions and conventional finite element analysis with sub-modeling are presented by Barut et al.[31]

The coupling of the global element with conventional elements is achieved by using the super element option of ANSYS. The ANSYS program is used to extract the form of the super element stiffness matrix and the force vector corresponding to the part of the region modeled by the global element. A well-established "super element" procedure is explained by Kohnke.[34] In this procedure, ANSYS creates an external file (SUB file) associated with the super element containing its stiffness matrix and force vector, with a known binary format. The global element stiffness matrix and force vector are evaluated to replace the corresponding entities in the SUB file. During solution, ANSYS reads in the SUB file and obtains the solution with the new stiffness matrix and force vector. The procedure for using global elements in ANSYS involves the development of pre- and post-processor routines as macro files. The pre-processor permits the replacement of the conventional elements in regions of high-stress concentration with a single global (super) element. This global element has the same number of nodes and nodal positions as those of the conventional elements it replaces. The post-processor initializes the database of results within the global element and displays the initialized values.

Along the common boundary of the global and conventional elements, the stresses associated with the global element are expressed in terms of the interface displacements. A typical coupling of the inner and outer regions is shown in Fig. 1. The interface between global and conventional elements is denoted by Γ. Because the global element satisfies the inter-element compatibility along the interface, the displacement continuity is enforced as

$$\mathbf{u}_\Gamma^c = \mathbf{u}_\Gamma^g \tag{3}$$

where the subscript Γ denotes the quantities associated with the interface and the superscripts c and g are used to distinguish the quantities belonging to the conventional finite elements and the global element, respectively.

The system of equations is expressed as

$$\mathbf{K}\,\mathbf{u} = \mathbf{F} \tag{4}$$

which can be partitioned into sub-matrices according to their association with the interface as

$$\begin{bmatrix} \mathbf{K}_c(\mathbf{u}_c) & \mathbf{K}_{cg}(\mathbf{u}_c) \\ \mathbf{K}_{gc}(\mathbf{u}_c) & \mathbf{K}_g \end{bmatrix} \begin{Bmatrix} \mathbf{u}_c \\ \mathbf{u}_g \end{Bmatrix} = \begin{Bmatrix} \mathbf{F}_c \\ \mathbf{0} \end{Bmatrix} \tag{5}$$

in which the terms on the right-hand side of the equation contain the external loads. This non-linear system of equations is solved for the unknown displacements of the outer region, as well as for the interface displacements. Because the eccentric loading path may result in large bending deflections for a single-lap joint, the sub-matrices $\mathbf{K}_c(\mathbf{u}_c)$, $\mathbf{K}_{cg}(\mathbf{u}_c)$, and $\mathbf{K}_{gc}(\mathbf{u}_c)$ in Eq. (5) arise from the geometrically nonlinear behavior of the conventional elements while the sub-matrix, $\mathbf{K}_g$ for the global element corresponds to the geometrically linear behavior. It is worth noting that during the iterative solution procedure the contribution from the global element remains the same. The conventional elements are four-noded, two-dimensional quadrilaterals with two degrees of freedom, u_x and u_y at each node. Next, the interface displacements are substituted back into the system of equations for the global element in order to solve for the singular stresses and the stress intensity factors. A sharp corner or a crack causes, in theory, an infinite stress concentration, often referred to mathematically as a singularity. Although such infinite stress values do not exist, the strength of the singular stress captures the effects of adhesive edge configurations as well as combinations of dissimilar materials.

Based on the concept of stress intensity factors, the generalized stress intensity factors K_1 and K_2 were introduced by Gradin[35] and Gradin and Groth[36] for the failure prediction of an adhesive bi-material interface as

$$K_1 + iK_2 = (2\pi)^{-\lambda_1} \lim_{r\to 0}\left[\sigma_{\theta\theta}(r,\theta=\theta^*;\lambda_1) - i\sigma_{r\theta}(r,\theta=\theta^*;\lambda_1)\right] \quad (6)$$

in which θ^* indicates the angular position of the interface. In the case of a crack $\theta^* = \pi$, the stress intensity factor values at the crack tip are calculated by invoking Eq. (1)

$$K_1 + i\,K_2 = (2\pi)^{-\lambda_1} \times [F_{\theta\theta}(\theta;\lambda_1) - i\,F_{r\theta}(\theta;\lambda_1)]_{\theta=\pi} \quad (7)$$

Based on this criterion, the bi-material joint always fails along the interface when the generalized stress intensity factors reach their experimentally measured critical values for specified edge configuration and material combinations. However, this type of criterion lacks an acceptable physical interpretation because the critical values for the generalized stress intensity factors are dependent on the material properties and geometry. In other words, the generalized stress intensity factors do not have a simple interpretation, as in the case of a crack in a homogeneous material. In the absence of a crack, a more meaningful parameter may be based on the energy rather than the stress intensity factors.

The energy stored in an element of a continuum can be decomposed into two components: dilatational and distortional. The dilatational component produces volume change, and the distortional component produces shape change. Failure initiation is associated with the dilatational component, which tends to produce voids or crack nucleations when it reaches a sufficient magnitude. The distortional component is responsible for local yielding of the material, which corresponds to material damage at a lower level of length scale.

The strain energy density failure criterion introduced by Sih[37] identifies regions in a material where the strain energy associated with dilatation is predominant over the energy associated with distortion. Regions of this type are susceptible to crack initiation and subsequent failure of the system. Unlike the classical application of fracture mechanics based on the energy release rate or stress intensity factor concept, which requires a knowledge of the size and location of the initial flaw, the strain energy density criterion determines the location of failure and the allowable load without assuming the existence of an initial flaw. The underlying assumptions and extensive applications of this criterion are presented by Sih.[38] With k representing a specific sector, the strain energy density function defined by

$$\frac{dW}{dV}(r,\theta) = \sum_{k=1}^{K}\left(\frac{dW}{dV}\right)^k \quad (8)$$

is not a continuous function. The strain energy density exhibits a stepwise change across the interface because of the discontinuous normal stresses at the interface. The strain energy density function representing the interface can be defined as the average value belonging to both sides of the interface

$$\frac{dW}{dV} = \frac{1}{2}\left[\frac{dW}{dV}\left(r,\theta^+\right) + \frac{dW}{dV}\left(r,\theta^-\right)\right] \quad (9)$$

in which the superscripts denote the two distinct sides of the interface. The failure initiation at the interface may occur when this averaged value reaches its critical value, $(dW/dV)_{cr}$, which is determined experimentally for a particular adhesive edge-type and material combination. If the adhesive failure mode is assumed, then the critical value is the same for all junctions of the joints that have the same adherends. Thus, a crack is more likely to initiate at locations that have the highest-valued strain energy density, and grow along the interface near the critical point.

At the possible failure sites, cracks are introduced in order to apply the concept of fracture mechanics. Specifically, the energy release rate is used to capture the effect of the adhesive edge configuration on the failure load. The energy release rate, G, at each crack tip is calculated by calculating the *J*-integral based on the expression

$$G = J = \sum_{k=1}^{K}\int_{\theta_k}^{\theta_{k+1}}\left[\left(\frac{dW}{dV}\right)^{(k)} n_x^{(k)} - (t_x^{(k)}u_{x,x}^{(k)} + t_y^{(k)}u_{y,x}^{(k)})\right]\varepsilon\, d\theta \quad (10)$$

where $(dW/dV)^{(k)}$ is the strain energy density, $t_\alpha^{(k)} = \sigma_{\alpha\beta}^{(k)} n_\beta^{(k)}$ $(\alpha,\beta = 1,2)$ are the tractions along the boundary of the integration path, $u_{x,x}^{(k)}$ and $u_{y,x}^{(k)}$ are the partial displacements of the global element with respect to local *x*-coordinate evaluated along the path of integration, and ε is a small radial distance between the junction and the circular path of integration that is associated with the k^{th} sector within the global element.

Numerical Results

The finite element representation of each lap-joint configuration with global and conventional elements evaluated in this study is illustrated in Fig. 3.

Square-end fillet

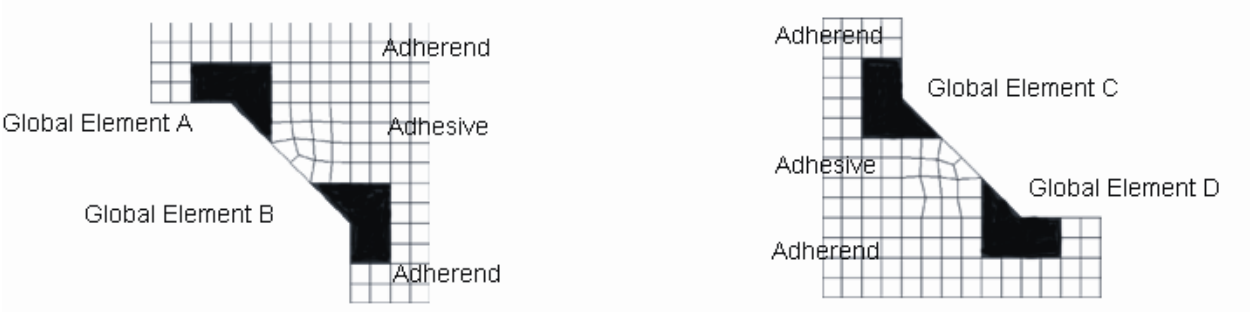

Chamfered-end fillet

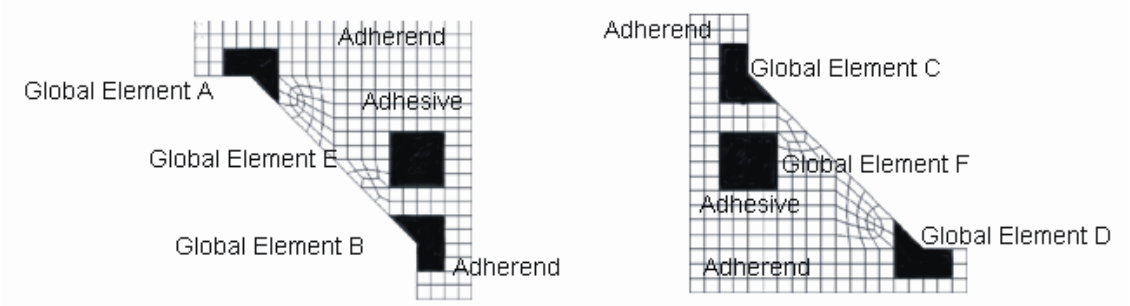

Spew fillet

Fig. 3 Finite element discretization with global and conventional elements: square-end fillet; chamfered-end fillet ; spew fillet.

A typical scaled deformation of one of the single-lap joints subjected to a specified load of $\sigma_0 = 1.0$ MPa is shown in Fig. 4. Because of the load eccentricity, relatively large rotations are present, thus relieving the bending moment at the end of the joint.

Fig. 4 Typical scaled overall deformation of single lap joint.

The leading-order eigenvalues retained in the construction of the interpolation functions for each global element of the lap joints with a square-end fillet, chamfered-end fillet, or spew fillet configuration are presented in Table 1. These eigenvalues are in agreement with those obtained by Destuynder et al.[24] The strength of the singularity (leading eigenvalue) in each adhesive end-type is significantly different. The results presented in Table 1 are obtained with the global element configurations shown in Fig. 3. The stresses are captured by retaining 12 eigenvalues in their series representations. Due to the presence of anti-symmetry, it suffices to show the results in global elements A and C in the lap joints with the square-end fillet and chamfered-end fillet, and in global elements A and F with the spew fillet.

Table 1 The strength of singularity in each global element

	Global Element	Strength
Square-end fillet	A, D	-0.3272
	B,C	-0.3015
Chamfered-end fillet	A,D	-0.02193
	B,C	-0.4147
Spew-fillet	A,B,C,D	-0.02193
	E,F	-0.3695

The negative values of the order (strength) of singularity arise from the presence of material and geometric discontinuities in the lap joint, thus leading to singular stresses in accordance with Eq. (1). As expected, the degree of geometric discontinuity has a significant effect on the strength of the singularity in the stress field. Based on the strength of the singular stresses of the three configurations, crack initiation is most likely to occur in the chamfered-end fillet configuration at junction C. The next likely failure site is in the spew fillet configuration at junction F. The square-end fillet appears to be the best design for an adhesive end configuration.

The global-local finite element results are also compared against the finite element analysis predictions with an extremely refined mesh of only conventional elements using ANSYS. In the finite element analysis with conventional elements only, the sub-modeling feature of ANSYS is utilized to achieve an acceptable mesh refinement near the junction. In the sub-modeling phase, the region of the global element consisted of approximately 13,000 to 67,000 elements, depending on the junction geometry. The comparisons of the results for the normalized peel and shear stresses along the adhesive-adherend interface in each global element of the square-end, chamfered-end, and spew fillet configurations are presented in Figs. 5-7, respectively. As observed in these figures, the predictions from the present global-local finite element analysis and the finite element analysis with an extremely refined mesh are in remarkable agreement up to a very small distance away from the junction point.

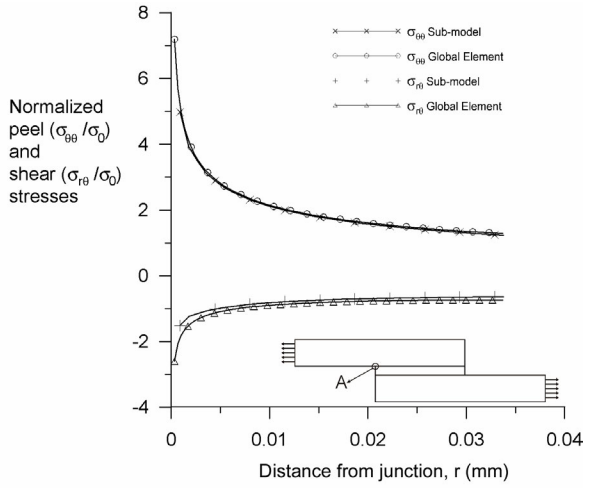

Junction A

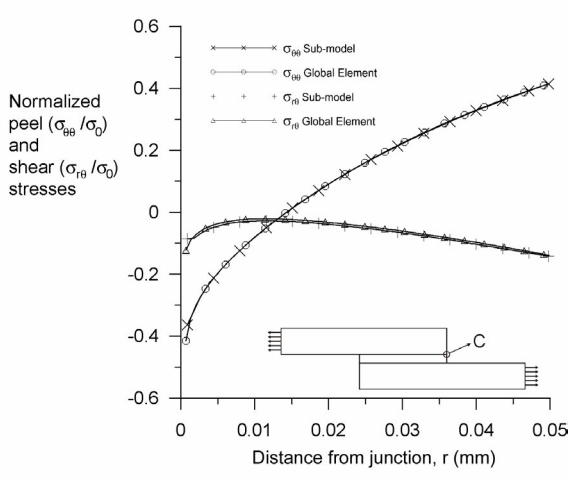

Junction C

Fig. 5 Comparison of stresses from sub-modeling and global element analyses for square-end fillet: junction A; junction C.

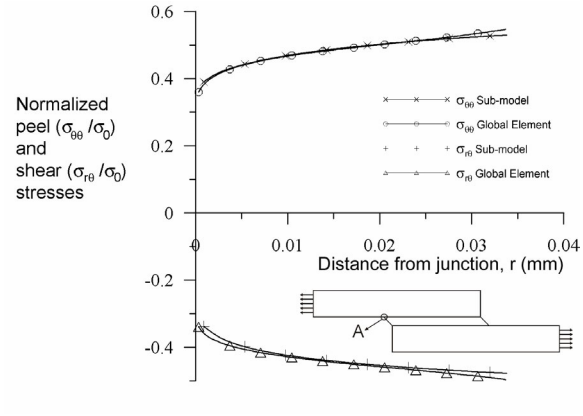

Junction A

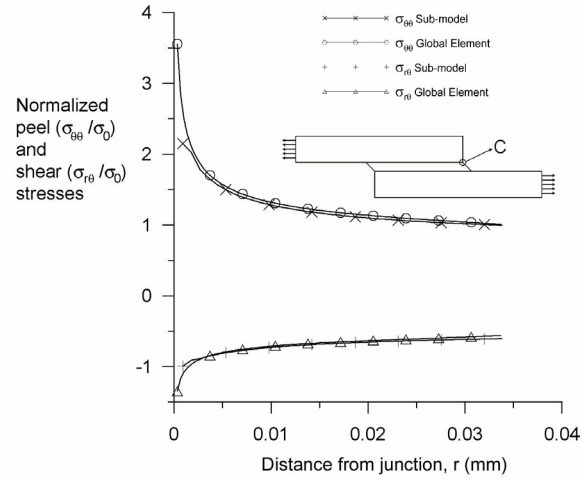

Junction C

Fig. 6 Comparison of stresses from sub-modeling and global element analyses for a chamfered-end fillet: junction A; junction C

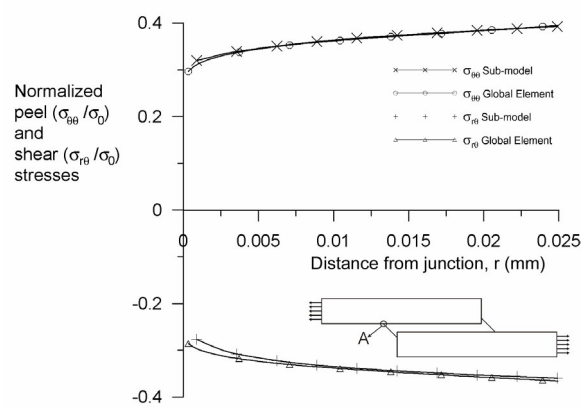

Junction A

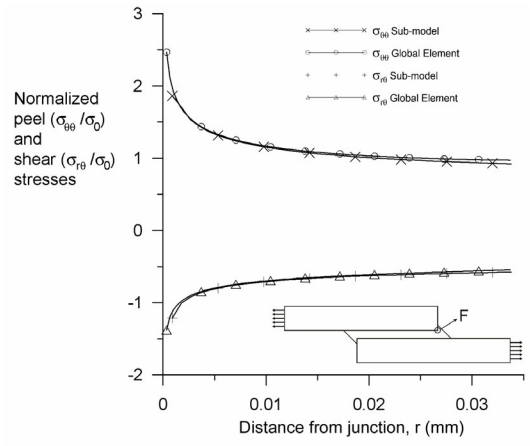

Junction C

Fig. 7 Comparison of stresses from sub-modeling and global element analyses for a spew fillet: junction A; junction F

The previous study by Blanchard and Watson[38] has confirmed that the results of a conventional finite element analysis are inaccurate at a point very close to the junction.

Along the adhesive-adherend interface, these stress components are highly non-symmetric as shown in Figs. 8-10. As shown in these figures, the stress field along the bond line is rather uniform away from the junctions (corners). The stresses increase across the overlap region as the ends of the bond line are approached. At the junctions where the highest order of singularity exists, both the peel and shear stresses exhibit a strong singular behavior. At the other junction, where the strength of the singularity is not as strong, these stresses reach their finite maximum value at a short distance from the end, and both the peel and shear stresses change direction.

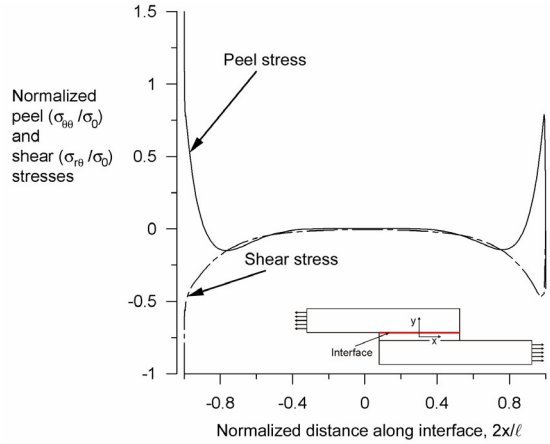

Fig. 8 Peel and shear stress distributions along the interface of a single-lap joint with a square-end fillet.

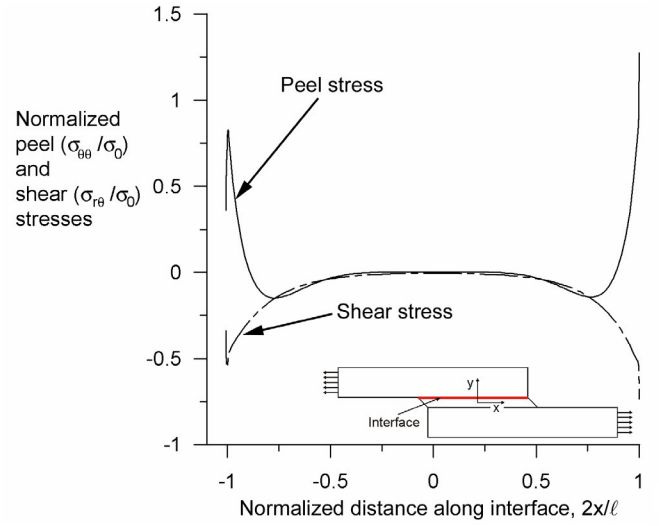

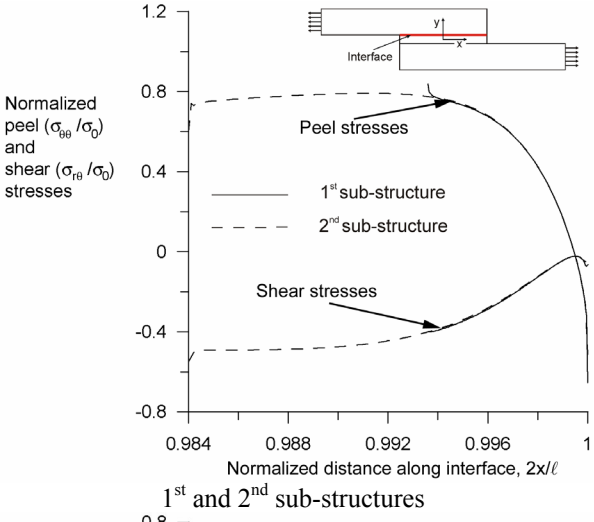

Fig. 9 Peel and shear stress distribution along the interface of a single-lap joint with a chamfered-end fillet.

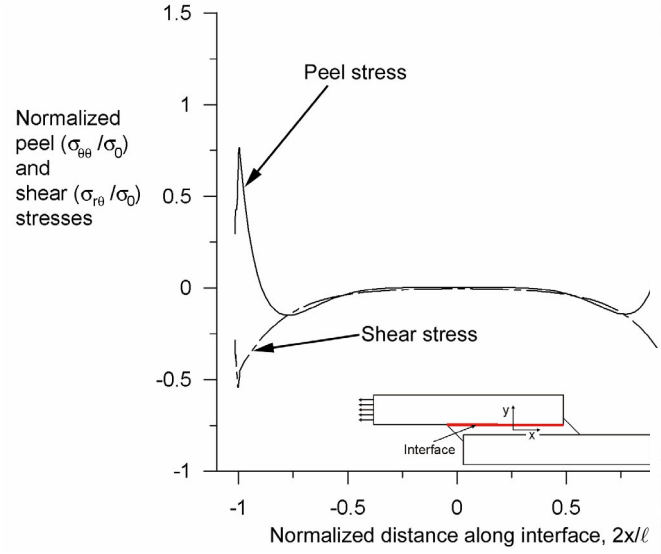

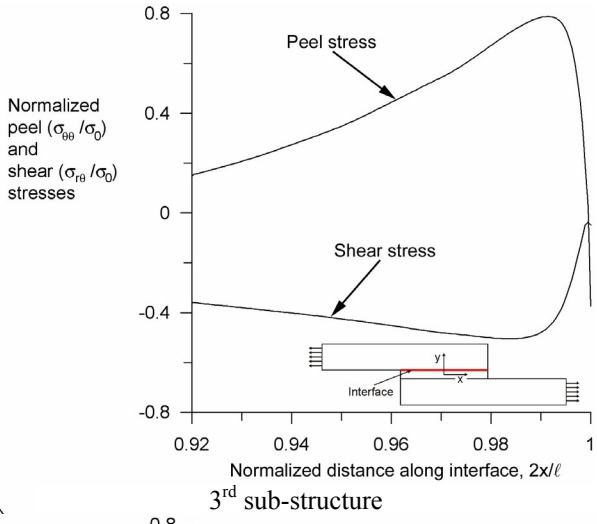

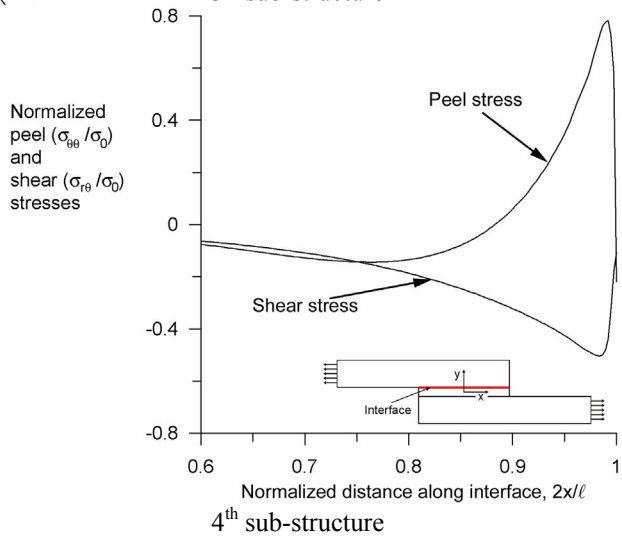

Fig. 10 Peel and shear stress distributions along the interface of a single-lap joint with a spew fillet.

Fig. 11 Behavior of stresses near junction C : 1st and 2nd sub-structures; 3rd sub-structure; 4th substructure

The rapid change in the stress field occurs so that the equilibrium equations are satisfied while imposing the continuity of traction and displacement components along the bond line and requiring traction free condition on the free surfaces. The validity of this behavior is confirmed by modeling the square-end fillet lap-joint *without* the use of a global element, instead four sub-structuring models with an extreme mesh refinement are employed to investigate the behavior of stresses at junction C. The region of sub-structuring analysis is rectangular with a height of $4h/5$ above and below the bond line. Its width along the bond line is varied as

$4h/5, 2h, 10h$ and $50h$ from junction C. In the first sub-structuring analysis, the element length in the vertical direction and along the bond line is specified as $2h/375$. In the subsequent sub-structures, the element length in the vertical direction is specified as $4h/375$. In the second, third and fourth sub-structures, the element length along the bond line is specified as $h/75, h/15$ and $h/3$. As shown in Figure 11a, the stresses along the bond line near junction C of square-end fillet obtained from the first and second sub-structuring analysis have identical values. The behavior of stresses also along the bond line obtained from the third and fourth sub-structuring is shown in Figure 11b-c. These results confirm the peculiar singular behavior, shown in Figures 8-10, at the junctions where both the peel and shear stresses change direction.

The negative peel stress results in pinching of the adhesive, thus impeding possible crack initiation. Because these stresses all possess mathematical singularity at the junctions, they do not provide information as to which end configuration either promotes or impedes premature failure. An examination of the strain energy density function around the junction points, shown in Figs. 12-14, at a specified distance of 0.0003 mm provides the possible failure sites. The results shown in these figures indicate that adhesive overflow drastically decreases the strain energy density level in the adhesive but not in the adherends. Based on the average strain energy density values for the interfaces in accordance with Eq. (9), failure is most likely to initiate along the interface at junction A of the square-end fillet. The next likely failure interface is at junction C of the chamfered-end fillet, and the interface associated with the spew fillet adhesive end is the best configuration.

The presence of an adhesive overflow clearly shifts the most critical site from junction C of the chamfered-end fillet configuration based on the strength of the singular stresses to junction A of the square-end fillet configuration. Failure initiation at junction A is consistent with the experimental observations presented by Le Gall et al.[39] The highest order of the stress singularity associated with these junction points does not predict this experimental observation.

According to the strain energy density criterion, a crack is likely to initiate at junction A of the square-end fillet, junction C of the chamfered-end fillet, and junction F of the spew fillet, and the crack is likely to grow along the interface. In order to capture the effect of the adhesive end configuration on the failure load, the energy release rate, G, at each crack tip is obtained by calculating the *J*-integral within the global element around the crack tip. As shown in Figs. 14a-b, an edge crack of length $0.1h$ is introduced at junction A of the square-end and chamfered-end configurations at junction C. At junction F of the spew fillet, the crack is situated along both the vertical and horizontal bond lines, forming a corner crack with length $0.2h$, shown in Fig. 14c. The associated energy release rates for each of these cracks are presented in Table 2.

Table 2 The energy release rate values at crack tips

	Crack Location	Energy Release Rate $(\mathrm{N/mm})$
Square-end fillet	A	0.307×10^{-4}
Chamfered-end fillet	C	0.162×10^{-4}
Spew-fillet	F	0.125×10^{-4} (Horizontal)
		0.104×10^{-4} (Vertical)

As shown in this table, the spew fillet configuration significantly improves the failure load (strength). For the sake of completeness, the stress intensity factors at each crack tip is presented in Table 3

Table 3 The stress intensity factors at crack tips.

	Crack Location	Stress Intensity Factors $(\mathrm{N/mm^2})\sqrt{\mathrm{mm}}$
		$K_1 + iK_2$
Square-end fillet	A	$0.399 + i\,0.294$
Chamfered-end fillet	C	$0.356 + i\,0.057$
Spew-fillet	F	$0.304 + i\,0.086$ (Horizontal)
		$0.267 + i\,0.108$ (Vertical)

Conclusions

Application of a global-local finite element technique that accounts for the singular behavior at junctions of dissimilar materials common to bonded single-lap joints is presented in this study. The global-local finite element approach eliminates the use of a fine mesh and provides a robust description of the stress field in the critical regions of the bonded lap joints. The influence of the adhesive overflow on the stress state is presented in terms of the strength of the singular stress field and the variation of the strain energy density at these junctions. The order of the singularity is not sufficient for predicting failure sites. Specific to the joint configuration in this study, the presence of adhesive overflow reduces peel stress, which is beneficial in improving failure load or strength. Adhesive overflow has a significant impact on the stress reduction in single-lap joints and should be

included in the stress analysis of single-lap joints. In conjunction with the strain energy density criterion and the concept of energy release rate, this capability may serve as a design tool to identify the effects of geometric and materials parameters on potential failure sites and failure loading.

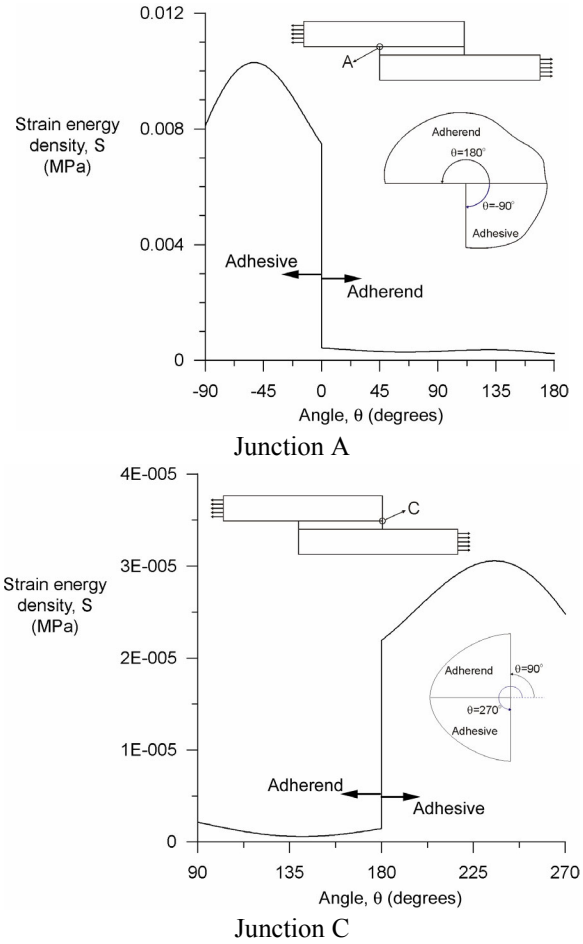

Fig. 12 Angular variation of strain energy at junction A and junction C of a square-end fillet

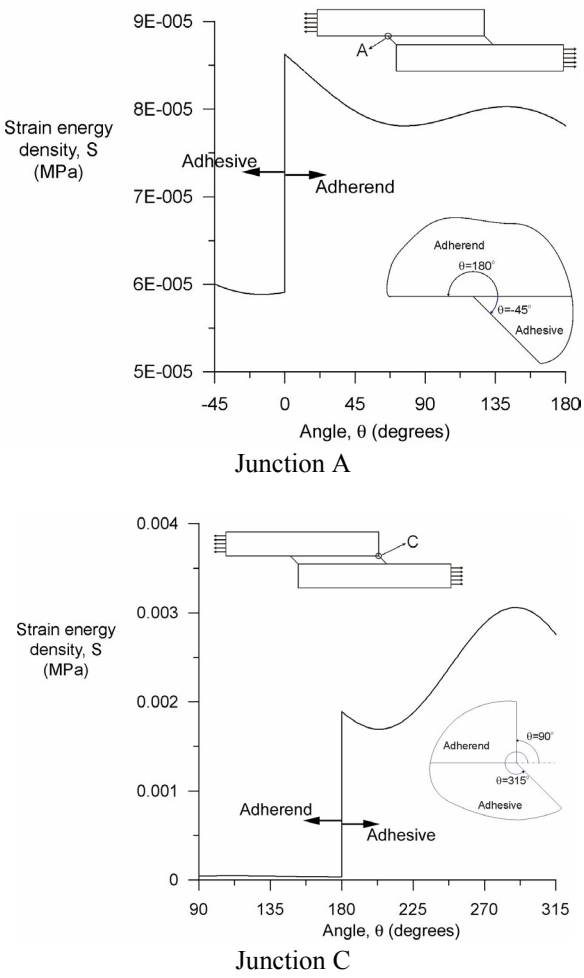

Fig.13 Angular variation of strain energy at junction A and junction C of a chamfered-end fillet

References

[1]Lang, T. P., and Mallick, P. K., "Effect of Spew Geometry on Stresses in Single Lap Adhesive Joints," *International Journal of Adhesion and Adhesives*, Vol. 18, 1998, pp. 167-177.

[2]Osnes, H., and Andersen, A., "Computational Analysis of Geometric Nonlinear Effects in Adhesivly Bonded Single Lap Composite Joints," *Composites: Part B*, Vol. 34, 2003, pp. 417-427.

[3]Pires, I., Quintino, L., Durodola, J. F., and Beevers, A., "Performance of Bi-adhesive Bonded Aluminum Lap Joints," *International Journal of Adhesion and Adhesives*, Vol. 23, 2003, pp. 215-223.

[4]Turaga, U. V. R. S., and Sun, C. T., "An Investigation of Adhesive Single-Lap Joints with Attachments," AIAA Paper 2003-1957, April, 2003.

[5]Goland, M., and Reissner, E., "The Stresses in Cemented Joints," *Journal of Applied Mechanics*, Vol. 66, 1944, pp. A17-A27.

[6]Dattaguru, B., Everett, R. A., Jr., Whitcomb, J. D, and Johnson, W. S., "Geometrically Nonlinear Analysis of Adhesively Bonded Joints," *Journal of Engineering Materials and Technology*, Vol. 106, 1984, pp. 59-65.

[7]Reddy, J. N., and Roy, S., "Non-Linear Analysis of Adhesively Bonded Joints," *International Journal of Non-Linear Mechanics*, Vol. 23, 1988, pp. 97-112.

[8]Pandey, P. C., Shankaragouda, H., and Singh, A. K., "Nonlinear Analysis of Adhesively Bonded Lap Joints Considering Viscoplasticity in Adhesives," *Computers and Structures*, Vol. 70, 1999, pp. 387-413.

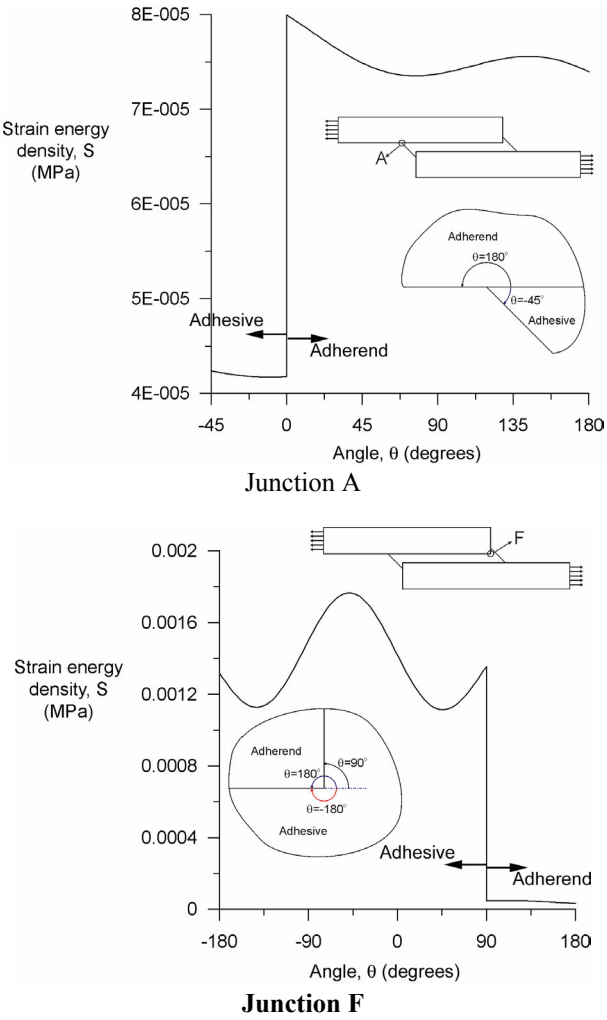

Fig. 14 Angular variation of strain energy at junction A and junction F of a spew fillet

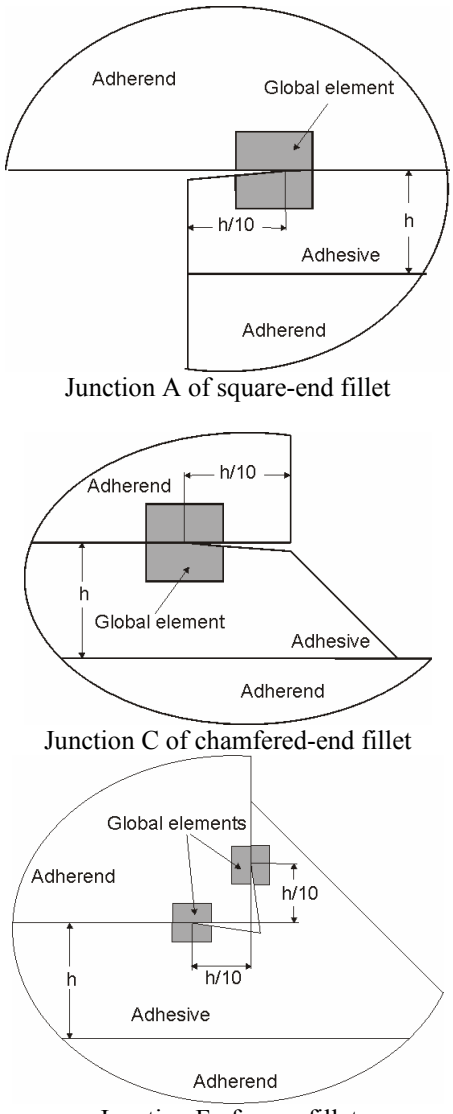

Fig. 15 Crack configurations at possible failure sites at junction A of a square-end fillet, junction C of a chamfered-end fillet, and junction F of a spew fillet

[9]Apalak, M. K., and Gunes, R., "On Non-Linear Thermal Stresses in an Adhesively Bonded Single Lap Joint," *Computers and Structures*, Vol. 80, 2001, pp. 85-98.

[10]Barsoum, R. S., "Application of the Finite Element Iterative Method to the Eigenvalue Problem of a Crack Between Dissimilar Media," *International Journal for Numerical Methods in Engineering*, Vol. 26, 1988, pp. 541-554.

[11]Barsoum, R. S., "Theoretical Basis of the Finite Element Iterative Method for the Eigenvalue Problem in Stationary Cracks," *International Journal for Numerical Methods in Engineering*, Vol. 26, 1988, pp. 531-539.

[12]Barsoum, R. S., "Asymptotic Fields at Interfaces Using the Finite Element Iterative Method," *Computers and Structures*, Vol. 35, 1990, pp. 285-292.

[13]Ding, S., and Kumosa, M., "Singular Stress Behavior at an Adhesive Interface Corner," *Engineering Fracture Mechanics*, Vol. 47, 1994, pp. 503-519.

[14]Ding, S., Miikisho, L., and Kumosa, M., "Analysis of Stress Singular Fields at a Bimaterial Wedge Corner," *Engineering and Fracture Mechanics*, Vol. 47, 1994, pp. 569-585.

[15]Mote, C. D., "Global-Local Finite Element," *International Journal of Numerical Methods in Engineering*, Vol. 3, 1971, pp. 565-574.

[16]Lin, K. N., and Mar, J. W., "Finite Element Analysis of Stress Intensity Factors for Cracks at a Bi-Material Interface," *International Journal of Fracture*, Vol. 12, 1976, pp. 521-531.

[17]Bradford, L. G., Dong, S. B., Nicol, D. A. C., and Westmann, R. A., "Application of Global-Local Finite Element Method to Fracture Mechanics," Technical Report, EPRI NP-239, Electric Power Research Institute, Palo Alto, 1976.

[18]Bradford, L. G., Dong, S. B., Tessler, A., and Westmann, R. A., "GLASS-II: Global-Local Finite Element Analysis," Technical Report, EPRI NP-1089, Electric Power Research Institute, Palo Alto, 1979.

[19]Bradford, L. G., Dong, S. B., Nicol, D. A. C., Westmann, R. A., "A Central Crack Element in Fracture Mechanics," *International Journal of Fracture*, Vol. 24, 1984, pp. 197-207.

[20]Dong, S. B., "Global-Local Finite Element Methods," *State-of-the-Art Surveys in Finite Element Technology* (A. K. Noor and W. D. Pilkey, Eds.), pp. 452-474, ASME, New York, 1983.

[21]Chen, E. P., "Finite Element Analysis of Bi-Material Interface Crack," *Theoretical and Applied Fracture Mechanics*, Vol. 3, 1985, pp. 257-262.

[22]Her, S., "Fracture Mechanics of Interface Cracks Between Dissimilar Anisotropic Materials," Ph.D. dissertation, University of California, Los Angeles, 1990.

[23]Munz, D., and Yang, Y., "Stress Singularities at the Interface in Bonded Dissimilar Materials under Mechanical and Thermal Loading," *ASME Journal of Applied Mechanics*, Vol. 35, 1992, pp. 460-473.

[24]Destuynder, P., Micavila, F., Santos, A., and Ousset, Y., "Some Theoretical Aspects in Computational Analysis of Adhesive Lap Joints," *International Journal for Numerical Methods in Engineering*, Vol. 35, 1992, pp. 1237-1262.

[25]Gadi, K. S., Joseph, P. F., and Kaya, A. C., "Enriched Finite Elements for a Crack Tip Touching an Interface," *Proceedings of the ASME Materials Division*, Vol.-I, MD-Vol. 69-1, pp. 257-263, IMEC&E, Los Angeles, 1995.

[26]Pageau, S. S., and Biggers, S. B., Jr., "Enriched Finite Elements for Regions with Multiple, Interacting Singular Fields," *AIAA Journal*, Vol. 34, 1996, pp. 1927-1933.

[27]Pageau, S. S., and Biggers, S. B., Jr., "Enrichment of Finite Elements with Numerical Solutions for Singular Stress Fields," *International Journal of Numerical Methods in* Engineering, Vol. 40, 1997, pp. 2693-2713.

[28]Akisanya, A. R., and Fleck, N.A., "Interfacial Cracking from the Free-Edge of a Long Bi-Material Strip," *International Journal of Solids and Structures*, Vol. 34, 1997, pp. 1645-1665.

[29]Madenci, E., Shkarayev, S., and Sergeev, B., "Thermo-Mechanical Stresses for a Triple Junction of Dissimilar Materials: Global-Local Finite Element Analysis," *Theoretical and Applied Fracture Mechanics*, Vol. 30, 1998, pp. 103-117.

[30]Qian, Z. Q., and Akisanya, A. R., "Wedge Corner Stress Behavior of Bonded Dissimilar Materials," *Theoretical and Applied Fracture Mechanics*, Vol. 32, 1999, pp. 209-222.

[31]Barut, A., Guven, I., and Madenci, E., "Analysis of Singular Stress Fields at Junctions of Multiple Dissimilar Materials under Mechanical and Thermal Loading," *International Journal of Solids and Structures*, Vol. 38, 2001, pp. 9077-9109.

[32]Sih, G. C., and Macdonald, B., "Fracture Mechanics Applied to Engineering Problems—Strain Energy Density Fracture Criterion," *Engineering Fracture Mechanics*, Vol. 6, 1974, pp. 361-386.

[33]Williams, M.L., "Stress Singularities Resulting from Various Boundary Conditions in Angular Corners of Plates in Extension," *ASME Journal of Applied Mechanics*, Vol. 19, 1952, pp. 526-528.

[34]Kohnke, P. (Ed.), *ANSYS Procedures Manual, Release 5.4*. ANSYS, Inc., Canonsburg, PA, 1998.

[35]Gradin, P. A., "A Fracture Initiation for Edge-Bonded Bimaterial Bodies," *Journal of Composite Materials,* Vol. 16, 1982, pp. 448-456.

[36]Gradin, P.A., and Groth, H.S., "A Fracture Criterion for Adhesive Joints in Terms of Material Induced Singularity," *Proceedings of the Third International Conference on Numerical Methods in Fracture Mechanics,* Pineridge Press, Swansea, UK, 1984, pp. 448-456.

[37]Sih, G. C., "Some Basic Problems in Fracture Mechanics and New Concepts," *Engineering Fracture Mechanics*, Vol. 5, 1973, pp. 365-377.

[38]Sih, G. C., *Mechanics of Fracture Initiation and Propagation*, Kluwer Academic Publishers, Dordrecht, The Netherlands, 1991.

[39]Blanchard, P. J. and Watson, R. D., "Residual Stresses in Bonded Armor Tiles for In-Vessel Fusion Components," *Nucl. Eng. Des*., Vol. 4, 1986, pp. 61-66.

[40]Le Gall, A. C., Jianmin, Q., and McDowell, D. L., "Delamination Cracking in Encapsulated Flip Chips," *46th Electronic Components and Technology Conference Proceedings,* IEEE, Piscataway, NJ, 1961, pp. 430-434.